NASA TECHNICAL NOTE

NASA TN D-5675

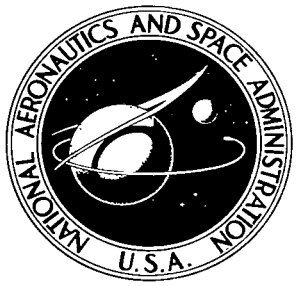

c. 1

NASA TN D-5675

0132529

TECH LIBRARY KAFB, NM

LOAN COPY: RETURN TO
AFWL (WLOL)
KIRTLAND AFB, N MEX

DIRECT MEASUREMENTS OF TURBULENT SKIN FRICTION ON A NONADIABATIC FLAT PLATE AT MACH NUMBER 6.5 AND COMPARISONS WITH EIGHT THEORIES

by Edward J. Hopkins, Earl R. Keener, and Pearl T. Louie

Ames Research Center
Moffett Field, Calif.

NATIONAL AERONAUTICS AND SPACE ADMINISTRATION • WASHINGTON, D. C. • FEBRUARY 1970

TECH LIBRARY KAFB, NM

0132529

1. Report No.	2. Government Accession No.	3. Recipient's Catalog No.
NASA TN D-5675		

4. Title and Subtitle

DIRECT MEASUREMENTS OF TURBULENT SKIN FRICTION ON A NONADIABATIC FLAT PLATE AT MACH NUMBER 6.5 AND COMPARISONS WITH EIGHT THEORIES

5. Report Date
February 1970

6. Performing Organization Code

7. Author(s)
Edward J. Hopkins, Earl R. Keener, and Pearl T. Louie

8. Performing Organization Report No.
A-3295

9. Performing Organization Name and Address
NASA Ames Research Center
Moffett Field, California 94035

10. Work Unit No.
129-01-08-24-00-21

11. Contract or Grant No.

13. Type of Report and Period Covered
Technical Note

12. Sponsoring Agency Name and Address
National Aeronautics and Space Administration
Washington, D.C. 20546

14. Sponsoring Agency Code

15. Supplementary Notes

16. Abstract

The local turbulent skin friction was directly measured with a floating-element balance mounted flush in a sharp-edged flat plate. The Mach number was 6.5, the length Reynolds number ranged from about 0.7 to 14 million, and the ratio of wall-to-adiabatic-wall temperature ranged from 0.3 to 0.5. The skin-friction results were used to evaluate eight theories on a generalized basis by determining which theory gives the best transformation of the data onto an incompressible skin-friction curve. The evaluation indicates that the best predictions of skin friction (within about 5 percent) are given by the Van Driest II or Coles theories when momentum-thickness Reynolds number is used. The uncertainty introduced by theories that require estimates of a virtual origin of turbulent flow is demonstrated.

17. Key Words Suggested by Author(s)

Hypersonic turbulent skin friction
Hypersonic turbulent boundary layer
Virtual origin of turbulent flow
Turbulent skin friction on nonadiabatic flat plates

18. Distribution Statement
Unclassified - Unlimited

19. Security Classif. (of this report)	20. Security Classif. (of this page)	21. No. of Pages	22. Price*
Unclassified	Unclassified	34	$3.00

*For sale by the Clearinghouse for Federal Scientific and Technical Information
Springfield, Virginia 22151

NOTATION

C_f	local skin-friction coefficient, $\frac{\tau_w}{q_e}$
C_F	average skin-friction coefficient, $\frac{2\theta}{x}$
M	Mach number
p	pressure
q	dynamic pressure, $\frac{1}{2}\rho U^2$
r	temperature recovery factor, $\frac{T_{aw} - T_e}{T_{t,e} - T_e} = 0.88$
$\mathfrak{R}$	gas constant for air, 1716 ft^2/sec^2 °R
R_x	Reynolds number based on distance to virtual origin of turbulent flow, $\frac{U_e}{\nu_e} x$
R_θ	Reynolds number based on momentum thickness, $\frac{U_e}{\nu_e}\theta$
T	temperature, °R
U	velocity
x	distance ahead of measuring station to virtual origin of turbulent flow
x_1	distance ahead of end of boundary-layer transition to either the leading edge or the virtual origin of turbulent flow
y	distance normal to flat plate
γ	ratio of specific heats
δ	boundary-layer thickness
θ	boundary-layer momentum thickness, $\int_0^\delta \frac{\rho U}{\rho_e U_e}\left(1 - \frac{U}{U_e}\right) dy$
μ	viscosity
ν	kinematic viscosity

ρ	mass density
τ	local shear stress
$(\bar{\ })$	variables in or transformed to a constant properties (incompressible) flow

Subscripts

aw	adiabatic-wall conditions
B	Baronti and Libby
C	Coles
E	Eckert
e	boundary-layer-edge conditions
H	Harkness
lam	laminar
M	Moore
o	reservoir conditions
SS	Sommer and Short
SC	Spalding and Chi
t	total conditions (isentropic stagnation)
turb	turbulent
VD	Van Driest
w	wall conditions
∞	free-stream conditions
2	behind normal shock wave

DIRECT MEASUREMENTS OF TURBULENT SKIN FRICTION ON A NONADIABATIC FLAT PLATE AT MACH NUMBER 6.5 AND COMPARISONS WITH EIGHT THEORIES

By Edward J. Hopkins, Earl R. Keener, and Pearl T. Louie

Ames Research Center

SUMMARY

The local turbulent skin friction was directly measured with a floating-element balance mounted flush in a sharp-edged flat plate. The Mach number was 6.5, the length Reynolds number ranged from about 0.7 to 14 million, and the ratio of wall-to-adiabatic-wall temperature ranged from 0.3 to 0.5. The skin-friction results were used to evaluate eight theories on a generalized basis by determining which theory gives the best transformation of the data onto an incompressible skin-friction curve. This evaluation indicates that the best predictions of skin friction (within about 5 percent) are given by the Van Driest II or Coles theories when momentum-thickness Reynolds number is used. The uncertainty introduced by theories that require estimates of a virtual origin of turbulent flow is demonstrated.

INTRODUCTION

Numerous direct and indirect measurements of turbulent skin friction have been made on flat plates in supersonic flow. Most of these data were compared in references 1 and 2 with predicted values from several skin-friction theories. From both reviews it can be concluded that satisfactory predictions of turbulent skin friction can be made for the adiabatic-wall case at supersonic Mach numbers up to about 4 by using either the reference temperature method of Sommer and Short (ref. 3) or the mixing-length methods of Wilson (ref. 4) and Van Driest II (ref. 5).

At hypersonic Mach numbers there is greater uncertainty regarding the proper method for predicting skin friction, both for the adiabatic-wall case (refs. 1, 2, and 6) and the nonadiabatic-wall case (refs. 7-9). Preliminary design studies on a possible first-generation Mach 6 cruise airplane indicate that the major part of the surfaces must be maintained below 1500° R; hence these surfaces will be cooled considerably below the adiabatic-wall temperature. In fact, the ratio of wall-to-adiabatic-wall temperature will probably range from about 0.4 to 0.5. For these flow conditions, the limited skin-friction data (most of which were obtained by indirect means) are inconclusive in showing the effects of heat transfer on the skin friction.

To make an accurate evaluation of existing methods for predicting skin friction at hypersonic Mach numbers, the present investigation was undertaken to provide direct measurements of skin friction on a flat plate having a local Mach number of 6.5. The ratio of wall-to-adiabatic-wall temperature of the plate was varied from 0.3 to 0.5. The momentum-thickness Reynolds number from boundary-layer surveys was used in the evaluation to avoid having to define arbitrarily the virtual origin of turbulent flow. The eight methods chosen for evaluation were those of Van Driest II (ref. 5), Spalding and Chi (ref. 9), Sommer and Short (ref. 3), Eckert (ref. 10), Moore (ref. 11), Harkness (ref. 12), Coles (ref. 13), and Baronti and Libby (ref. 14). A portion of this evaluation was reported in reference 15 without presenting the details of the analysis and measurements.

APPARATUS AND TEST

Wind Tunnel

The investigation was conducted in air in the Ames 3.5-Foot Hypersonic Wind Tunnel. This facility is a blow-down-type wind tunnel in which the air is heated by a hot pebble bed to temperatures ranging from about 1200° to 2000° R. The throat and nozzle walls are cooled by helium injection ahead of the throat, the helium remaining within the wind-tunnel boundary layer as confirmed by surveys. The Mach 7.4 nozzle was used in the present test. The stagnation pressure was varied from 7 to 66 atm and the testing time was between 2 and 3 min depending on the pressure level.

Model and Instrumentation

The model was a sharp-edged flat plate, which was sting supported as shown in figure 1. A dimensional sketch of the flat plate is presented in figure 2. The average thickness of the leading edge was 0.005 inch as measured on a magnetometer. The boundary layer was surveyed at a station 39.2 in. behind the leading edge with a pitot-pressure probe, a static-pressure probe, and a total-temperature probe. Details of these probes are shown in figures 3 and 4. The boundary-layer survey complex and its side supports can be seen near the rear of the plate in figure 1. After the survey mechanism was stopped, sufficient time was allowed for the pressures to attain equilibrium. The total-temperature probe had only a single shield to minimize its size and possible interference effects from interaction of the probe shock and the boundary layer. The temperature probe was calibrated over a range of tunnel unit Reynolds numbers that covered those encountered within the boundary layer.

The skin friction was measured by a floating-element balance (manufactured by Kistler Instrument Corporation), which had a movable element 0.370 in. in diameter and a perimetrical gap of 0.003 in. This element was centered by means of a self-nulling circuit for each measurement. A photograph of the balance with the water jacket used to maintain the electrical

portion of the balance below 200° F is shown in figure 5. The balance was calibrated by hanging small weights from its surface oriented in a vertical plane.

Test Conditions

The sharp-edged flat plate was mounted with its test surface 3° to the windward so that the local Mach number was 6.5 for a free-stream Mach number of 7.4. Local unit Reynolds numbers varied from about 0.2 to 4.1 million per foot. Static-pressure measurements made on the surface indicated nearly isobaric conditions in the vicinity of the survey station. Nearly isothermal wall conditions were maintained along the centerline of the plate by water cooling near the leading edge and air cooling in the instrument housing. The large mass of the aluminum flat plate also assisted in maintaining nearly isothermal conditions (within 50° F), verified by monitoring thermocouples along the length of the plate. The increase in surface temperature during a run was less than 5 percent of the total temperature.

For low Reynolds numbers it was necessary to trip the boundary layer to obtain fully developed turbulent flow at the survey station. This was accomplished by a row of pentagonal trips placed 4 in. behind the leading edge as shown in figures 1 and 2. Effectiveness of the trips was verified by the sublimation visual-flow technique. Fluorene was chosen as the sublimable material and was sprayed on the model in a solution of petroleum ether.

Measurements

The following quantities were measured:

Free stream:

Reservoir total pressure, $p_{t,o}$

Reservoir total temperature, $T_{t,o}$

Average Mach number at the plate leading-edge station obtained from tunnel survey without model installed, M_∞

Flow angle from a tunnel survey without model installed

Flat plate:

Surface temperature, T_w

Local shear stress, τ_w

Boundary-layer survey:

Pitot pressure, $p_{t,2}$

Total temperature (indicated), T_t

Distance from surface to center of probe faces, y

DATA REDUCTION

Boundary-Layer-Edge Conditions

Local flow conditions at the edge of the boundary layer on the flat plate (39 in. behind the leading edge) were calculated from the measured boundary-layer-edge pitot pressure ($p_{t,2}$), reservoir total pressure ($p_{t,o}$), reservoir total temperature ($T_{t,o}$), and the tunnel calibration Mach number (M_∞). The compressible flow relations in reference 16 were used in the calculations, which included corrections for calorically imperfect gas effects.

Static pressure.- Since the test surface was mounted 3° to the windward, the static pressure (p_e) was calculated for a flow deflection angle of 3°. Measured surface pressures agreed with the calculated pressures within ±5 percent for the higher Reynolds numbers ($R_\theta > 4000$).

Mach number.- Mach number ($M_e = 6.5 \pm 0.17$) was calculated from the Rayleigh pitot equation using the calculated p_e and the measured pitot pressure from the traversing probe. There was no difficulty in picking an edge condition from the pitot-probe measurements at the survey station. The real gas correction for Mach number was less than 1 percent for the temperature range of the test.

Static temperature.- Static temperature (T_e) was calculated from M_e and $T_{t,e}$, assuming that $T_{t,e} = T_{t,o}$. A real gas correction was applied to the ratio of $T_e/T_{t,e}$. This static temperature was used to calculate velocity (U_e) from the equation $U_e = M_e\sqrt{\gamma \Re T_e}$ ($\gamma = 1.4$ since $T_e < 300°$ R), density (ρ_e) from the equation of state ($\rho_e = p_e/\Re T_e$), and viscosity (μ_e) from Keyes' equation (ref. 17) and table 1 (eq. (38)).

Dynamic pressure.- The dynamic pressure was calculated from $q_e = [q_e/(p_{t,2})_e](p_{t,2})_e$. For $5 < M_e < 10$ and $T_{t,e} < 2000°$ R, the ratio $q_e/(p_{t,2})_e = 0.54$ is within 1 percent as discussed in reference 18. Consequently, the accuracy of q_e depends primarily on the accuracy of $(p_{t,2})_e$.

Momentum Thickness

The momentum thickness (θ) of the boundary layer was obtained by integration from

$$\theta = \int_0^{\delta} \frac{\rho U}{\rho_e U_e}\left(1 - \frac{U}{U_e}\right) dy$$

The ratios ρ/ρ_e and U/U_e were determined from the measured pitot-pressure survey, the calculated surface static pressure (p_e), and an assumed linear Crocco distribution of total temperature with velocity (unit Prandtl no.) as follows: From the perfect gas equation, with static pressure assumed constant across the boundary layer, the density ratio may be written as:

$$\frac{\rho}{\rho_e} = \frac{T_e}{T} = \left(\frac{1 + 0.2M^2}{1 + 0.2M_e^2}\right)\frac{T_{t,e}}{T_t}$$

and the velocity ratio may be written in terms of Mach number and temperature ratio as

$$\frac{U}{U_e} = \frac{M}{M_e}\left[\left(\frac{1 + 0.2M_e^2}{1 + 0.2M^2}\right)\frac{T_t}{T_{t,e}}\right]^{1/2}$$

The local Mach number was calculated from the Rayleigh pitot equation, given p_e and the measured $p_{t,2}$. The ratio $T_t/T_{t,e}$ was calculated from the Crocco relation in the following form:

$$\frac{T_t}{T_{t,e}} = \left[\left(C^2 + \frac{T_w}{T_{t,e}}\right)^{1/2} + C\right]^2$$

where

$$C = 0.5\left(1 - \frac{T_w}{T_{t,e}}\right)\left(\frac{1 + 0.2M_e^2}{1 + 0.2M^2}\right)^{1/2}\frac{M}{M_e}$$

Real gas corrections to the density and velocity ratios were found to be small and were ignored.

Total temperatures were measured for four of the boundary-layer surveys; the results agreed with the Crocco temperature distribution within experimental accuracy (ref. 15). Since measured temperatures were not available for all the data, the Crocco temperature relation was used for all the calculations.

ACCURACY

The estimated probable uncertainties of the pertinent recorded and calculated quantities are as follows:

$T_{t,o}$	±50° R	$p_{t,2}$, q_e	±2 percent
T_w	±10° R	U_e/ν_e	±7 percent
p_e, T_w, θ	±5 percent	R_θ	±8 percent
M_e	±0.17	y	±0.005 in.

The manufacturer's specifications for the probable uncertainties in the measurements from the skin-friction balance are as follows:

Linearity deviation, percent of full scale	±0.3
Null stability, percent of full scale	±1

Additional information concerning the accuracy of a similar balance is reported in reference 8. No buoyancy correction was applied since a negligible pressure gradient was measured in the vicinity of the balance. Preliminary wind-tunnel tests of a special balance, geometrically similar to the force balance, indicated that the floating element is less than 100° F above the outer case. An important concern is the extent to which the floating element remains flush under heating. Previous experimenters using floating element have reported that the error caused by floating-element depression under 0.0005 in. is less than 2 percent. No protrusion can be tolerated. At room temperature, depression was well within 0.0005 in. During the time for traversing the boundary layer (2 to 3 min), the balance readings varied less than 2 percent, which indicated that the floating element was not protruding due to heating. Balance calibrations before and after the test, the zeroes, and test-coil calibrations taken between each test run were within the specifications. In conclusion, the probable error in wall shear stress is estimated to be ±2 percent of full-scale value or ±0.04 psf. The repeatability of the measured data during a boundary-layer survey was within ±2 percent (20 test points).

METHOD OF ANALYSIS

In practice, skin friction is most commonly calculated on the basis of a length Reynolds number R_x. In the usual case of mixed flow (combined laminar, transitional, and turbulent flow) the $C_f(R_x)$ method of data analysis requires the determination of a suitable virtual origin of turbulent flow so that an equivalent length of turbulent flow can be used in R_x. No direct method is available to determine the virtual origin, however, especially for the case of artificially tripped flow; consequently, the $C_f(R_x)$ method has some disadvantages in evaluating theories.

All the theories can be written as a function of either R_x or R_θ. The latter, based on momentum thickness, is a more meaningful boundary-layer Reynolds number for analyzing data and accounts for all the momentum losses within the boundary layer up the measuring station. The use of R_θ to correlate local skin friction is less arbitrary than the use of an assumed

virtual origin. As shown in reference 2, the $C_f(R_\theta)$ method of analysis, which is used here, satisfactorily correlates available measurements of adiabatic-wall skin friction at subsonic and supersonic Mach numbers.

Each of the eight theories examined herein contains functions for transforming the compressible skin friction onto the incompressible plane. Each method is evaluated on a generalized basis by determining how close a particular method transforms the measured C_f and R_θ onto an incompressible $\overline{C}_f$ vs. $\overline{R}_\theta$ curve. Such a comparison permits experimental points obtained under different test conditions to be examined together. It follows that if a given theory transforms experimental data onto the incompressible curve, that theory can be expected to account properly for the effects of M_e, T_w/T_{aw}, $T_{t,e}$, and R_θ on skin friction. It is also expected that a theory that transforms the experimental skin-friction data onto the incompressible curve ($\overline{C}_f$ vs. $\overline{R}_\theta$) would also accurately predict skin friction in terms of the Reynolds number based on the distance behind the virtual origin of turbulent flow to the measuring station. For this study, the transformed experimental points are compared with the Kármán-Schoenherr incompressible relationship of $\overline{C}_f$ with $\overline{R}_\theta$, defined by equation (39) in table 1. This equation is known to give a good representation of available experimental data over a wide range of Reynolds numbers (see refs. 19 and 20).

THEORIES

Equations for the eight theories evaluated are given in detail in table 1. All the theories are of the transformation type; that is, each theory contains transformation functions that establish a correspondence between compressible and incompressible skin friction. For some theories, the transformations were originally given for only C_f and R_x; the transformation for R_θ was obtained from the following relationship for a flat plate having isobaric and isothermal flow conditions (e.g., see ref. 9):

$$\frac{\overline{R}_\theta}{R_\theta} = \frac{\overline{C}_f}{C_f}\frac{\overline{R}_x}{R_x}$$

Van Driest II (Ref. 5)

The Von Kármán mixing length is used in the Prandtl shear-stress equation with the Crocco temperature distribution assumed through the boundary layer. It should be noted that a temperature recovery factor of 0.88 for turbulent flow was used in the equations for this theory in a manner given by Spalding and Chi (ref. 9).

Spalding and Chi (Ref. 9)

The function for transforming C_f (eq. (7)) was assumed to be the same as that derived by Van Driest with a temperature recovery factor included.

The transformation function for R_θ (eq. (8)) was assumed to comprise the factors $(T_w/T_{aw})^n$ and $(T_w/T_e)^m$ where n and m were derived from experimental data. Unfortunately, when this method was developed, few directly measured skin-friction data were available at the higher Mach numbers, so that m and n were primarily derived from indirect measurements of skin friction.

Sommer and Short (Ref. 3)

It is assumed that C_f and R_θ can be transformed to incompressible values, provided that the density and viscosity contained in these variables are evaluated at some reference temperature (eq. (11)) that is a function of M_e, T_w, and $T_{t,e}$. This reference-temperature (T') method was first proposed by Rubesin and Johnson for a laminar boundary layer in reference 21. The constants contained in this function were derived from limited experimental data obtained in a free-flight range.

Eckert (Ref. 10)

The reference temperature assumptions are the same as those for Sommer and Short's theory; however, the contants in the reference-temperature equation (eq. (14)) are different.

Moore (Ref. 11)

The adiabatic theory of Wilson (ref. 4), based on the Von Kármán mixing-length concept, is extended to include the effects of heat transfer. It assumes a quadratic total temperature-velocity relationship $(T_t - T_w)/(T_{t,e} - T_w) = (U/U_e)^2$. Reference 15 provides evidence that such a temperature distribution is valid only for wind-tunnel walls and not for flat plates.

Harkness (Ref. 12)

The mixing-length concept of Von Kármán is utilized in a manner similar to that of Van Driest II (ref. 5) except that the effect of heat transfer on the laminar sublayer is obtained from available experimental data.

Coles (Ref. 13)

A law of corresponding stations is hypothesized in which the product $C_f R_\theta$ is the same at corresponding points in any two flows related by the transformation. For the transformation, a substructure hypothesis is invoked with a constant substructure Reynolds number based on a density and viscosity evaluated at a suitable mean temperature, T_C (eq. (26)). Although Coles' theory implies that $(\overline{C}_f)_C$ is a function of $(\overline{C}_f\overline{R}_\theta)_C$, $(\overline{C}_f)_C$ also is given as a function of $(\overline{R}_\theta)_C$ for conformity with the other generalization presentations.

Baronti and Libby (Ref. 14)

The transformation is patterned after Coles except that it uses the sublayer hypothesis of Donaldson (ref. 22) instead of the substructure hypothesis chosen by Coles. The Reynolds number associated with the laminar sublayer is assumed invariant and to contain a density and viscosity that are based on the temperature at the edge of the laminar sublayer T_f (eq. (31)).

RESULTS AND DISCUSSION

Skin-Friction Data $C_f(R_\theta)$

The skin-friction data are presented in figure 6 as a function of R_θ and are tabulated in table 2 with the local flow conditions. The cross-hatched band in the figure represents the maximum expected spread of the experimental data from differences in the ratio T_w/T_{aw} according to Coles' theory. The dashed curve represents the expected level of the data according to the Rubesin-Johnson theory (ref. 21) for laminar flow. The results indicate that the three data points obtained at the lowest Reynolds numbers are probably for transitional flow and that the remaining data points are probably for turbulent flow.[1]

Evaluation of Theories

Figure 7 presents the turbulent data on a generalized basis $\bar{C}_f(\bar{R}_\theta)$ for each of the eight theories. Note that the data obtained with and without boundary-layer trips (indicated by flagged and unflagged symbols) generally are correlated on the basis of $\bar{R}_\theta$ for each theory. The boundary-layer trips increased the momentum-thickness Reynolds number (R_θ) as shown in table 2 and thereby moved the virtual origin of turbulent flow forward.

A comparison of the transformed data with the Kármán-Schoenherr incompressible curve indicates that the theories of both Van Driest II[2] (fig. 7(a)) and Coles (fig. 7(d)) would predict the skin friction to within about 5 percent. For all other theories, the transformed experimental points lie above the incompressible curve; consequently, the skin friction would be underpredicted by about 15 percent by the theory of Sommer and Short, and 20 to 25 percent by the theories of Spalding and Chi, Eckert, Harkness, and Baronti and Libby. Moore's theory, although based on an incorrect temperature distribution within the boundary layer (see Theories section), would give good predictions of skin friction at high Reynolds numbers but would underpredict the skin friction up to 10 percent at the lowest Reynolds numbers. See figure 7(c).

[1] Boundary-layer transition measurements obtained without trips are presented in reference 23; the results substantiate this conclusion.

[2] If a temperature recovery factor of 1.0 instead of 0.88 were used in the Van Driest theory, the predicted C_f would be about 5 percent lower and the correlations poorer.

A comparison of the results presented at the top and bottom of figures 7(d) and 7(e) indicates that the coordinates given by Coles' law of corresponding stations (i.e., $\bar{C}_f = f(\bar{C}_f\bar{R}_\theta)$ correlate the data about the same as those used for the other methods (i.e., $\bar{C}_f = f(\bar{R}_\theta)$).

VIRTUAL ORIGIN

Previous evaluations of skin friction have used primarily the $\bar{C}_f(\bar{R}_x)$ method of analysis, which requires the determination of a virtual origin of turbulent flow. It is of interest, therefore, to examine the location of the virtual origin as predicted by each of the eight theories for the measured value of R_θ. The calculation procedure is described in appendix A. The test condition chosen for the results (fig. 8) corresponds to the highest Reynolds number for which transition was natural (no trips). All the theories locate the virtual origin well ahead of the end of transition indicated by the sublimation studies of reference 23. The maximum difference in the distance from the measuring station to the virtual origin is less than 20 percent. Consequently, these differences in virtual origin cannot explain the large differences in the predicted C_f (fig. 7) which must arise primarily from differences in the transformation functions for each theory given in table 1. For example, the underprediction of C_f of 20 to 25 percent by the Spalding and Chi theory compared with a prediction within 5 percent by the Van Driest theory results from differences in the transformed R_θ of 200 to 250 percent for these theories as shown in figure 7(a).

Another method for obtaining the virtual origin is discussed in reference 24. This method assumes that $\theta_{lam} = \theta_{turb}$ at the end of transition so that the distance ahead of the end of transition to the virtual origin may be calculated from $x_{l,turb} = (C_{F,lam}/C_{F,turb})(x_{l,lam})$, where the average skin-friction ratio is determined from theory, and $x_{l,lam}$ is the distance to the leading edge. For the experimental case of figure 8, this method gives a value of $x = 23.5$ in., which is midway between the Van Driest II theory and the end of transition indicated by the sublimation studies.

Several other methods for obtaining the virtual origin are discussed in references 1 and 7. For heat-transfer models, the location of peak heating is frequently assumed to be the location of the virtual origin. This location corresponds approximately with the end of transition indicated by sublimation studies, as confirmed by a comparison of the sublimation studies on the present model (ref. 23) and the unpublished detailed temperature distribution on the Polek flat-plate model (ref. 15). The comparisons shown in figure 8 indicate that a virtual origin at peak heating is not consistent with the momentum-thickness measurements. Consequently, any evaluation of skin-friction or heat-transfer measurements based on such a choice for the virtual origin would lead to an entirely different and possibly erroneous choice of theory from that arrived at from the generalization analysis of figure 7.

In conclusion, the $\overline{C}_f(\overline{R}_\theta)$ method is recommended by the authors for the evaluation of skin-friction theories to avoid an arbitrary, and possibly incorrect, choice of the virtual origin of turbulent flow.

CONCLUDING REMARKS

Direct measurements of skin friction on a nonadiabatic flat plate at a Mach number of 6.5 indicate that the methods of both Van Driest II and Coles predict the skin friction within about 5 percent. Six other theories underpredict the skin friction as follows: Moore, 10 percent; Sommer and Short, 15 percent; Spalding and Chi, Eckert, Harkness, Baronti and Libby, 20 to 25 percent. The theories are evaluated on the basis of the measured momentum-thickness Reynolds number, and this method is shown to be consistent with the visual-flow studies for the end of transition. There is no noticeable effect of boundary-layer trips on the correlation other than to increase the momentum-thickness Reynolds number. Arbitrary selection of a virtual origin at the end of transition (near peak heating) is shown to be inconsistent with the momentum-thickness results. This approach can lead to entirely different and possibly erroneous conclusions regarding the best theory for predicting skin friction. It is suggested that additional direct measurements of skin friction be analyzed on the basis of measured momentum-thickness Reynolds number for a range of test variables wider than that of the present investigation before a final selection of a theory is made for predicting turbulent skin friction at hypersonic Mach numbers.

Ames Research Center
National Aeronautics and Space Administration
Moffett Field, Calif., 94035, Sept. 25, 1969

APPENDIX A

CALCULATION OF VIRTUAL ORIGIN OF TURBULENT FLOW

The procedure followed in calculating virtual origin from the measured R_θ is given below. Since each theory has different transformations for R_θ and C_f, it follows that each theory also will give different locations for the virtual origin.

From the Kármán-Schoenherr equations, the incompressible local skin-friction coefficient $\overline{C}_f$ can be written in terms of $\overline{C}_F$ (see ref. 25) or $\overline{R}_\theta$ (eq. (39), table 1). By equating these relationships for $\overline{C}_f$ and by substituting $2\overline{R}_\theta/\overline{R}_x$ for $\overline{C}_F$, a single equation is obtained in terms of $\overline{R}_\theta$ and $\overline{R}_x$ as

$$\frac{0.242(2\overline{R}_\theta/\overline{R}_x)}{0.242 + 0.8686\sqrt{2\overline{R}_\theta/\overline{R}_x}} = \frac{1}{17.08(\log_{10}\overline{R}_\theta)^2 + 25.11\log_{10}\overline{R}_\theta + 6.012} \tag{A1}$$

$\overline{R}_x$ can be determined by iteration from equation (A1) after substituting $\overline{R}_\theta = (R_\theta)(\overline{R}_\theta/R_\theta)$ in equation (A1); the ratio $\overline{R}_\theta/R_\theta$ is given in table 1. After $\overline{R}_x$ is found, R_x is calculated from

$$R_x = \overline{R}_x\left(\frac{\overline{C}_f}{C_f}\Big/\frac{\overline{R}_\theta}{R_\theta}\right) \tag{A2}$$

where $\overline{C}_f/C_f$ is also given in table 1. Finally, the distance from the survey station to the virtual origin of turbulent flow is calculated from

$$x = \frac{R_x}{U_e/\nu_e} \tag{A3}$$

REFERENCES

1. Peterson, John B., Jr.: A Comparison of Experimental and Theoretical Results for the Compressible Turbulent-Boundary-Layer Skin Friction With Zero Pressure Gradient. NASA TN D-1795, 1963.

2. Hopkins, Edward J.; and Keener, Earl R.: Study of Surface Pitots for Measuring Turbulent Skin Frction at Supersonic Mach Numbers - Adiabatic Wall. NASA TN D-3478, 1966.

3. Sommer, Simon C.; and Short, Barbara J.: Free-Flight Measurements of Turbulent Boundary-Layer Skin Friction in the Presence of Severe Aerodynamic Heating at Mach Numbers From 2.8 to 7.0. NACA TN 3391, 1955.

4. Wilson, R. E.: Turbulent Boundary-Layer Characteristics at Supersonic Speeds - Theory and Experiment. J. Aeron. Sci., vol. 17, no. 9, Sept. 1950, pp. 585-594.

5. Van Driest, E. R.: The Problem of Aerodynamic Heating. Aeron. Eng. Rev., vol. 15, no. 10, Oct. 1956, pp. 26-41.

6. Adcock, Jerry B.; Peterson, John B., Jr.; and McRee, Donald I.: Experimental Investigation of a Turbulent Boundary Layer at Mach 6, High Reynolds Numbers, and Zero Heat Transfer. NASA TN D-2907, 1965.

7. Bertram, Mitchel, H.; and Neal, Luther, Jr.: Recent Experiments in Hypersonic Turbulent Boundary Layers. AGARD Specialists Meeting on Recent Developments in Boundary-Layer Research, Naples, Italy, May 10-14, 1965.

8. Garringer, Darwin J.; and Saltzman, Edwin J.: Flight Demonstration of a Skin Friction Gage to a Local Mach Number of 4.9. NASA TN D-3830, 1967.

9. Spalding, D. B.; and Chi, S. W.: The Drag of a Compressible Turbulent Boundary Layer on a Smooth Flat Plate With and Without Heat Transfer. J. Fluid Mech., vol. 18, pt. 1, Jan. 1964, pp. 117-143.

10. Eckert, E. R. G.: Engineering Relations for Heat Transfer and Friction in High Velocity Laminar and Turbulent Boundary Layer Flow Over Surfaces With Constant Pressure and Temperature. Trans. ASME, vol. 78, no. 6, Aug. 1956, pp. 1273-1283. (Also available in J. Aeron. Sci., vol. 22, 1955, pp. 585-587.)

11. Moore, Dave R.: Velocity Similarity in the Compressible Turbulent Boundary Layer With Heat Transfer. Rep. DRL-480, CM 1014, Defense Res. Lab., Univ. of Texas, 1962.

12. Harkness, John L.: The Effect of Heat Transfer on Turbulent Boundary Layer Skin Friction. Rep. DRL-436, CM 940, Defense Res. Lab., Univ. of Texas, 1959.

13. Coles, Donald: The Turbulent Boundary Layer in a Compressible Fluid. Rand Corp. Rep. R-403-PR, 1962.

14. Baronti, P. O.; and Libby, P. A.: Velocity Profiles in Turbulent Compressible Boundary Layers. AIAA J., vol. 4, no. 2, Feb. 1966, pp. 193-202.

15. Hopkins, Edward J.; Rubesin, Morris W.; Inouye, Mamoru; Keener, Earl R.; Mateer, George C.; and Polek, Thomas E.: Summary and Correlation of Skin-Friction and Heat-Transfer Data for a Hypersonic Turbulent Boundary Layer on Simple Shapes. NASA TN D-5089, 1969.

16. Ames Research Staff: Equations, Tables, and Charts for Compressible Flow. NACA Rep. 1135, 1953. (Supersedes NACA TN 1428.)

17. Bertram, Mitchel H.: Comment on "Viscosity of Air." J. Spacecraft Rockets, vol. 4, no. 2, Feb. 1967, p. 287.

18. Cary, John P.; and Keener, Earl R.: Flight Evaluation of the X-15 Ball-Nose Flow-Direction Sensor as an Air-Data System. NASA TN D-2923, 1965.

19. Smith, Donald W.; and Walker, John H.: Skin-Friction Measurements in Incompressible Flow. NASA TR 26, 1959. (Supersedes NACA TN 4231.)

20. Locke, Frederick W. S., Jr.: Recommended Definition of Turbulent Friction in Incompressible Fluids. DR Rep. 1415, Navy Dept., Bureau of Aeronautics, Research Div., June 1952.

21. Rubesin, Morris W.; and Johnson, H. A.: A Critical Review of Skin Friction and Heat-Transfer Solutions of the Laminar Boundary Layer of a Flat Plate. Trans. ASME, vol. 71, no. 4, May 1949, pp. 383-388.

22. Donaldson, C. duP.: On the Form of the Turbulent Skin-Friction Law and Its Extension to Compressible Flows. NACA TN 2692, 1952.

23. Hopkins, Edward J.; and Keener, Earl R.: Unit Reynolds Number Effects on Boundary-Layer Transition at Mach 6. AIAA J., vol. 6, no. 5, May 1968, p. 956.

24. Wallace, J. E.; and McLaughlin, E. J.: Experimental Investigations of Hypersonic, Turbulent Flow and Laminar, Leeward-Side Flow on Flat Plates. Tech. Rep. AFFDL-TR-66-63, vol. I, Cornell Aeron. Lab., Inc., July 1966, pp. 23-24.

25. Schoenherr, Karl E.: Resistance of Flat Surfaces Moving Through a Fluid. Soc. Naval Architects and Marine Engr., vol. 40, 1932, pp. 279-313.

26. Coles, Donald: The Law of the Wall in Turbulent Shear Flow. 50 Jahre Grenzschichtforschung, H. Görtler and W. Tollmien, eds.; Friedr. Vieweg and Sohn, Braunschweig, 1955, pp. 153-163.

TABLE 1.- TRANSFORMATION FUNCTIONS

	Van Driest II (ref. 5)	Spalding-Chi (ref. 9)	Sommer-Short (ref. 3)	Eckert (ref. 10)	Moore (ref. 11)	Harkness (ref. 12)	Coles (ref. 13)	Baronti-Libby (ref. 14)
$\frac{\bar{C}_f}{C_f}$	$\frac{rm}{[\sin^{-1}\alpha+\sin^{-1}\beta]^2}$ (1)	$\frac{rm}{[\sin^{-1}\alpha+\sin^{-1}\beta]^2}$ (7)	$\frac{T'_{SS}}{T_e}$ (9)	$\frac{T'_E}{T_e}$ (12)	$\frac{\sigma F}{\lambda(\sin^{-1}\sqrt{\sigma})^2}$ (15)	$\frac{m}{\left[\frac{1+m-F}{P}-\sin^{-1}\left(\frac{1-m-F}{P}\right)\right]^2}$ (19)	$\frac{T_w\mu_C}{T_e\mu_w}$ (24)	$\frac{T_w\mu_B}{T_e\mu_w}$ (28)
$\frac{\bar{R}_\theta}{R_\theta}$	$\frac{\mu_e}{\mu_w}$ (2)	$\frac{1}{(F)^{0.702}(F_{aw})^{0.772}}$ (8)	$\frac{\mu_e}{\mu_{SS}}$ (10)	$\frac{\mu_e}{\mu'_E}$ (13)	$\frac{0.1156e^{0.4L}\mu_e}{L\mu_w}$ (16)	$\frac{0.1716\,\mu_e}{L\zeta\mu_w}$ (20)	$\frac{\mu_e}{\mu_C}$ (25)	$\frac{\mu_e}{\mu_B}$ (29)
Notation	$\alpha = \frac{2A^2-B}{\sqrt{4A^2+B^2}}$ (3) $\beta = \frac{B}{\sqrt{4A^2+B^2}}$ (4) $A = \sqrt{(rm)/F}$ (5) $B = \frac{1+rm-F}{F}$ (6)	α, β, A, and B are the same as for Van Driest II	$T'_{SS} = T_e \times [1+0.035M_e^2+0.45(F-1)]$ (11)	$T'_E = T_e \times [1+0.039M_e^2+0.50(F-1)]$ (14)	$\sigma = \frac{F-1}{F}$ (17) $\lambda = 0.9212 \times e^{0.0706\sigma}$ (18)	$\zeta = 2.566e^{\xi}$ (21) $\xi = -\frac{0.8953L\sqrt{mF}}{P}$ (22) $P = \sqrt{(1+m-F)^2+4mF}$ (23)	$T_C = \frac{T_e}{430}\int_0^{430}\left(\frac{T}{T_e}\right)_C d\bar{z}$ (26) $\frac{T}{T_e} = F+(1+m-F)\left(\frac{\bar{U}}{\bar{U}_\tau}\right)\sqrt{\frac{(\bar{C}_f)_C}{2}} - \left(\frac{\bar{U}}{\bar{U}_\tau}\right)^2 \frac{m(\bar{C}_f)_C}{2}$ (27)[a] $\left(\frac{\bar{U}}{\bar{U}_\tau}\right)$ given as a function of $\bar{z}$ in ref. 26 T_C is obtained from eqs. (24), (26), and (27) by iteration	$\mu_B = \left(\frac{T_f}{T_e}\right)(\mu_f)\left[F+(1+m-F)(5.3)\sqrt{\frac{(\bar{C}_f)_B}{2}} - m\frac{(\bar{C}_f)_B}{2}(37.45)\right]^{-1}$ (30) $T_f = T_e\left[F+(1+m-F)(10.6)\sqrt{\frac{(\bar{C}_f)_B}{2}} - m\frac{(\bar{C}_f)_B}{2}(10.6)^2\right]$ (31)[a] T_f is obtained from eqs. (28), (30), and (31) by iteration

where the common factors are:

$F = T_w/T_e$ (32)

$F_{aw} = T_w/T_{aw}$ (33)

$L = 11.5+6.6t$ (34)

$m = 0.2\,M_e^2$ (35)

$t = 1 - F_{aw}$ (36)

$T_{aw} = T_e(1 + rm)$ (37)

$r = 0.88$

$\mu = 0.0232\times10^{-6}\sqrt{T}\left(1 + \frac{220}{T}10^{-\frac{9}{T}}\right)^{-1}$ $\frac{\text{lb-sec}}{\text{ft}^2}$ (38)

(Keyes' viscosity formula, ref. 17)

T = temperature, °R

[a]Crocco temperature distribution for unit Prandtl number

and the Kármán - Schoenherr incompressible equation is

$$\bar{C}_f = \frac{1}{17.08\,(\log_{10}R_\theta)^2 + 25.11\log_{10}\bar{R}_\theta + 6.012} \quad (39)$$

TABLE 2.- FLOW CONDITIONS FOR SKIN-FRICTION DATA

Symbol	M_e	U_e, ft/sec	p_e, lb/ft^2	q_e, lb/ft^2	$(U_e/\nu_e)\times 10^{-6}$ ft^{-1}	$R_\theta \times 10^{-3}$	T_e, °R	T_w, °R	$T_{t,e}$ °R	T_w/T_{aw}	$C_f \times 10^3$	Condition of boundary layer	Boundary-layer trips
○	6.5	4557	22.0	650.4	1.697	2.262	205	583	1850	0.34	1.57	Turbulent	Off
□		3893	4.1	121.1	0.471	1.099	149	548	1379	0.37	1.38	Transitional	↓
△		4033	13.6	403.3	1.486	2.389	160	559	1474	0.41	1.52	Turbulent	↓
◇		4449	6.6	196.0	0.528	1.017	195	534	1770	0.32	1.24	Transitional	On
◺		4702	37.4	1105.1	2.615	4.555	218	587	1960	0.32	1.22	Turbulent	↓
▽		3939	14.0	415.0	1.644	3.300	153	551	1410	0.43	1.25		↓
◺		4037	21.5	636.3	2.367	5.900	161	564	1477	0.42	1.20		↓
▷		3888	23.0	683.0	2.822	3.815	149	561	1376	0.45	1.23		Off
◁		3550	8.1	238.3	1.263	2.185	124	537	1158	0.51	1.41		On
◁		3625	12.1	356.4	1.813	3.890	130	543	1250	0.50	1.35		↓
◺		3679	27.7	819.6	4.011	8.326	133	572	1240	0.51	1.00		↓
◺		3665	27.8	822.0	4.065	6.419	132	572	1231	0.51	1.06		Off
◇	↓	4652	3.6	106.4	0.241	0.728	213	545	1922	0.30	0.90	Transitional	↓

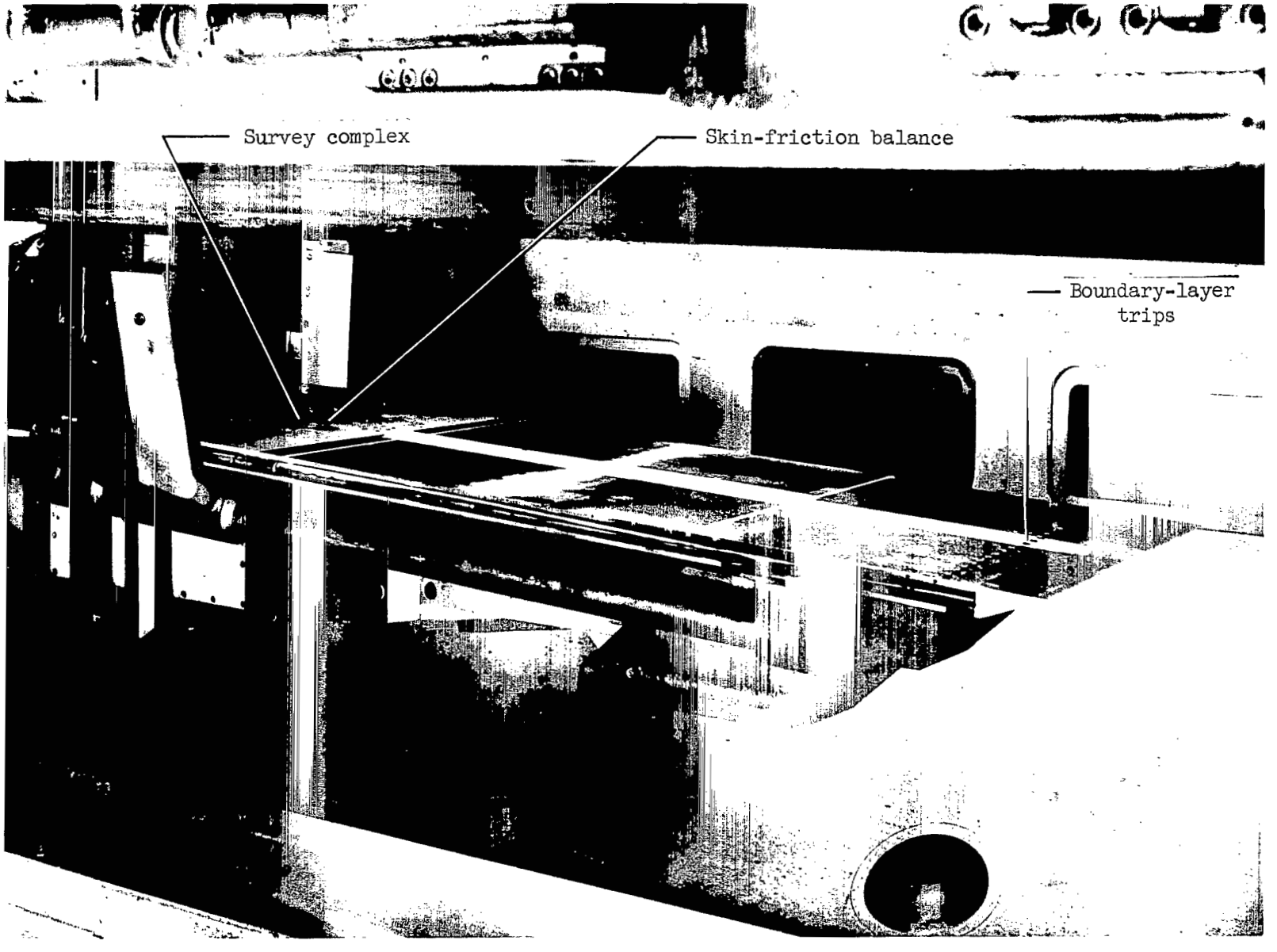

Figure 1.- Sharp-edged flat plate mounted in the Ames 3.5-Foot Hypersonic Wind Tunnel.

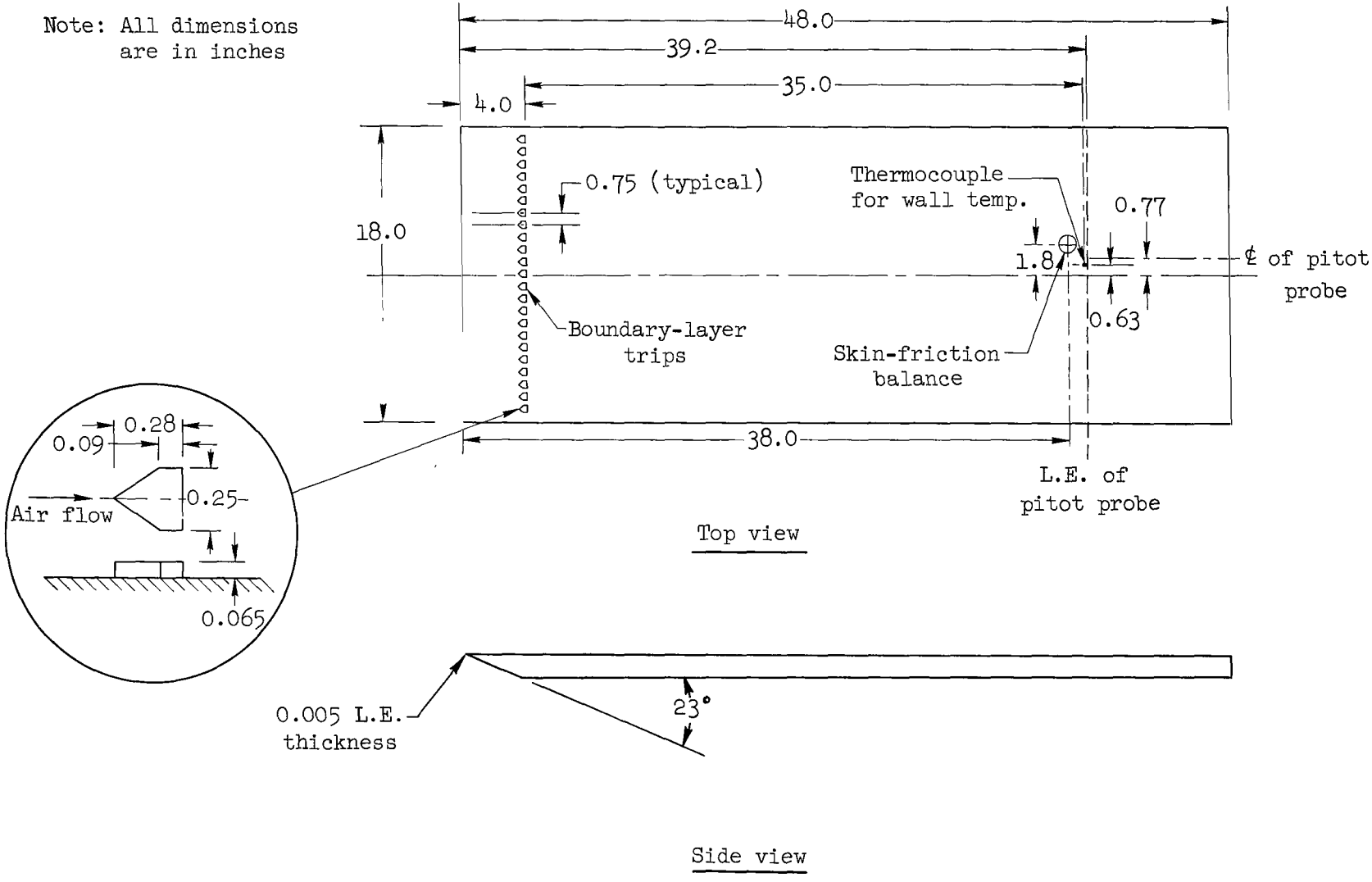

Figure 2.- Geometry of flat plate and other pertinent details.

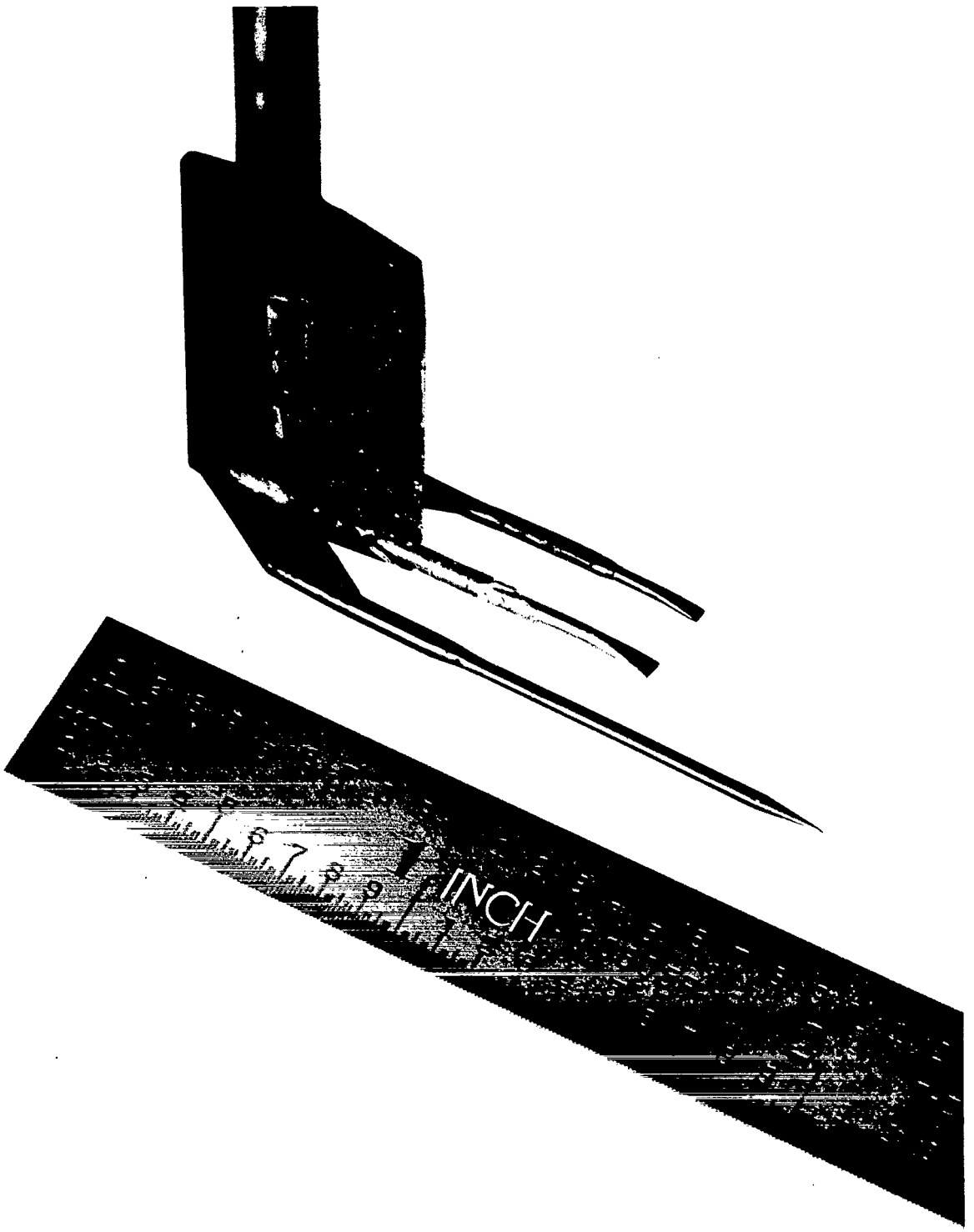

Figure 3.- Survey complex.

A-38502

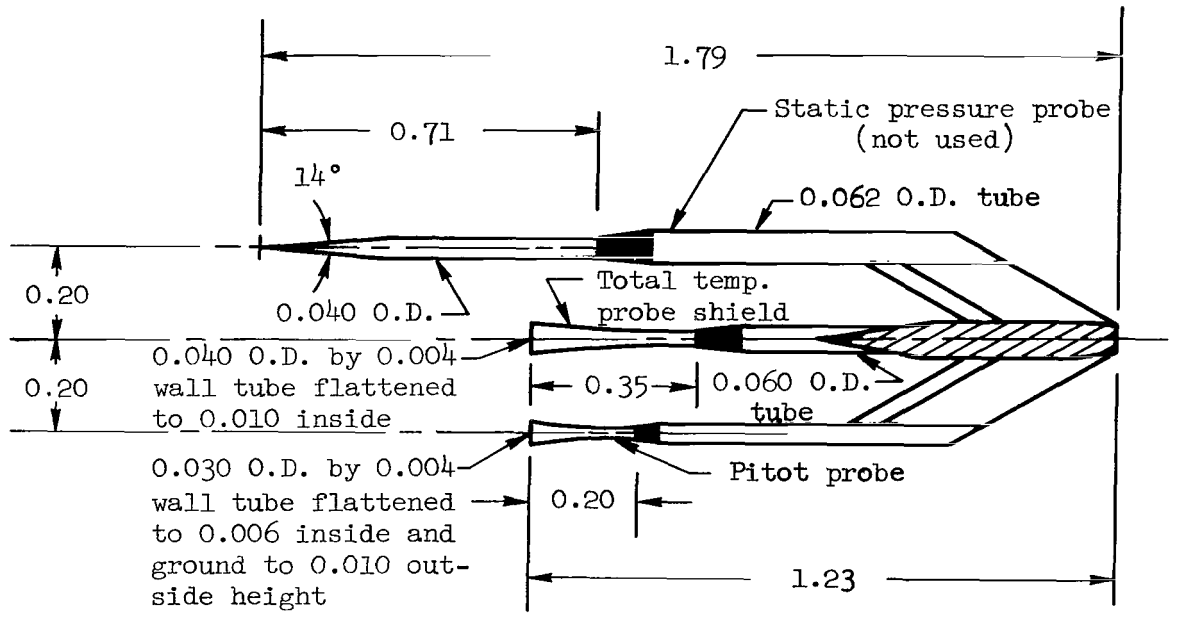

Top view

Note: All dimensions
are in inches

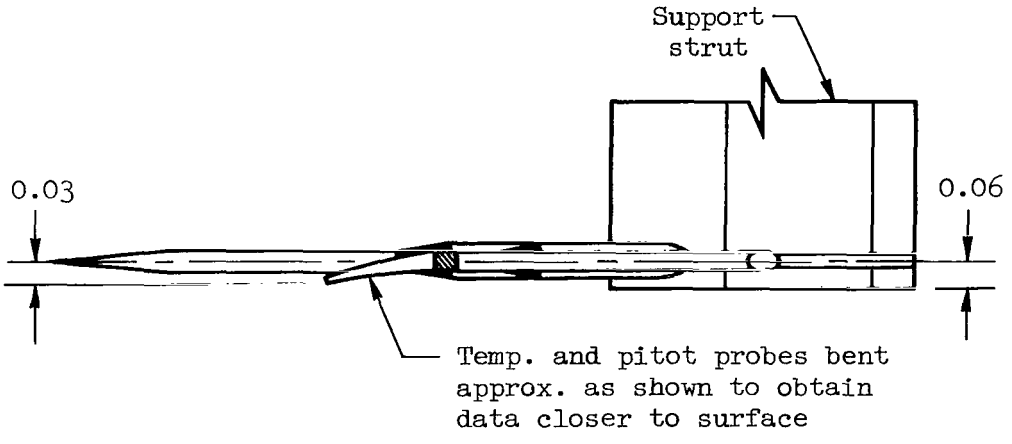

Side view

Figure 4.- Geometry of survey complex.

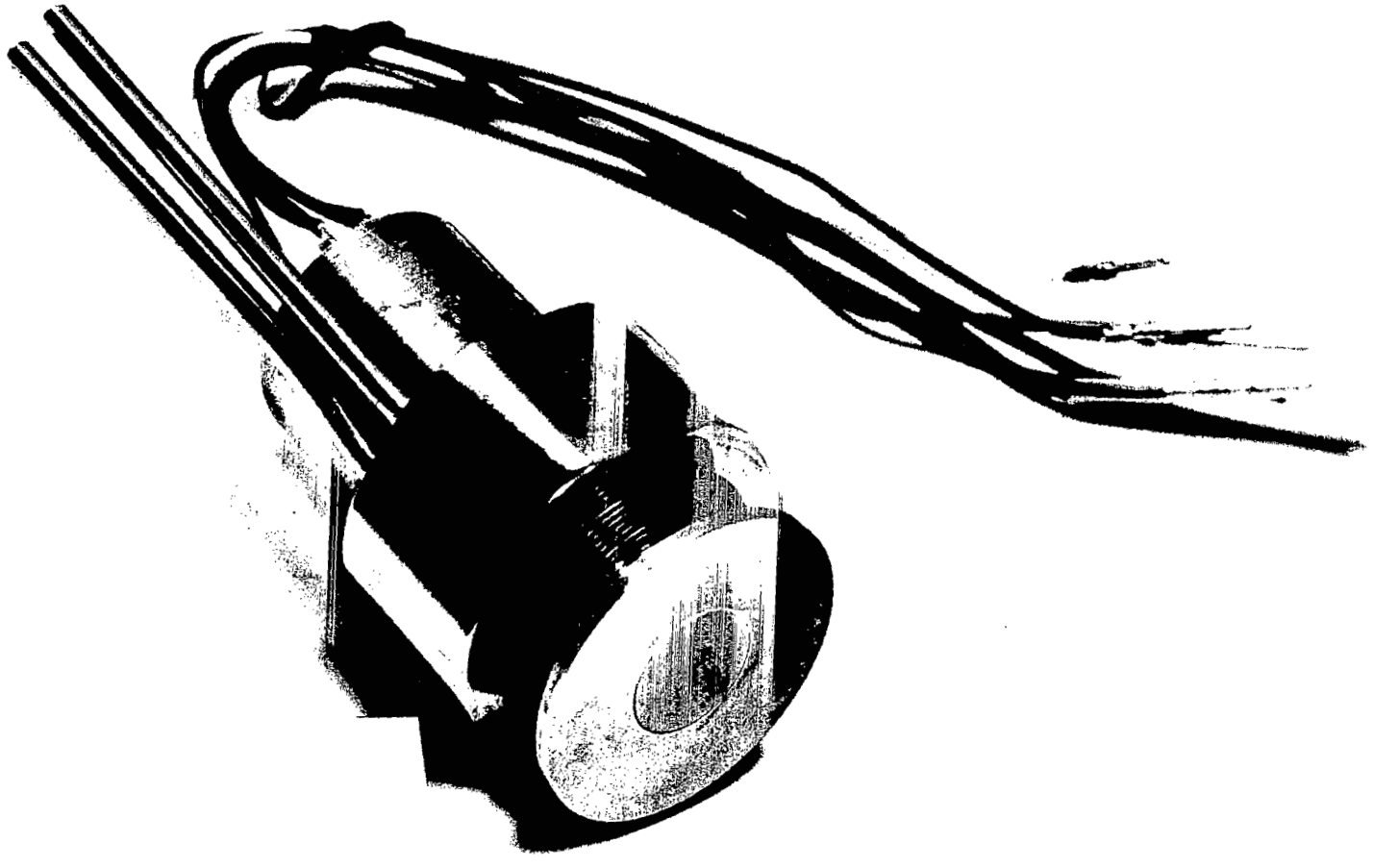

Figure 5.- Skin-friction balance.

A-39408

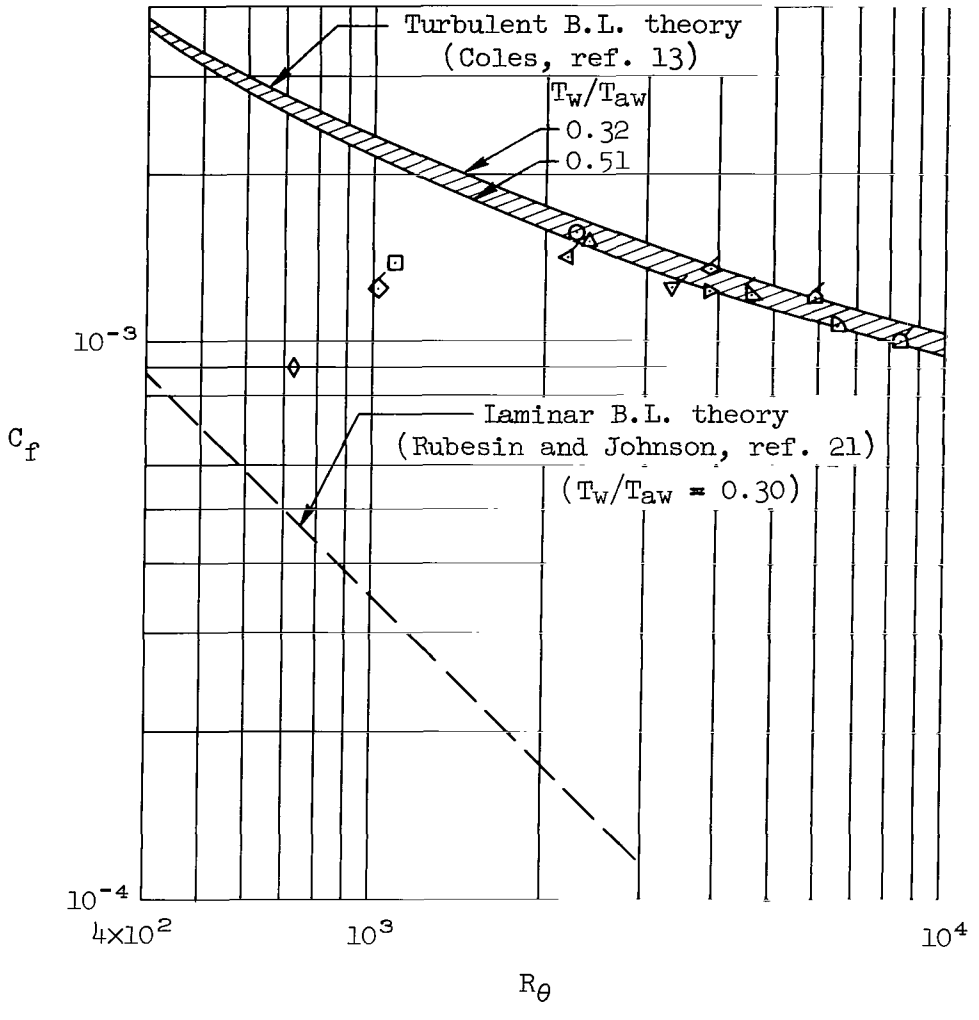

Figure 6.- Local skin-friction data (symbols defined in Table 2).

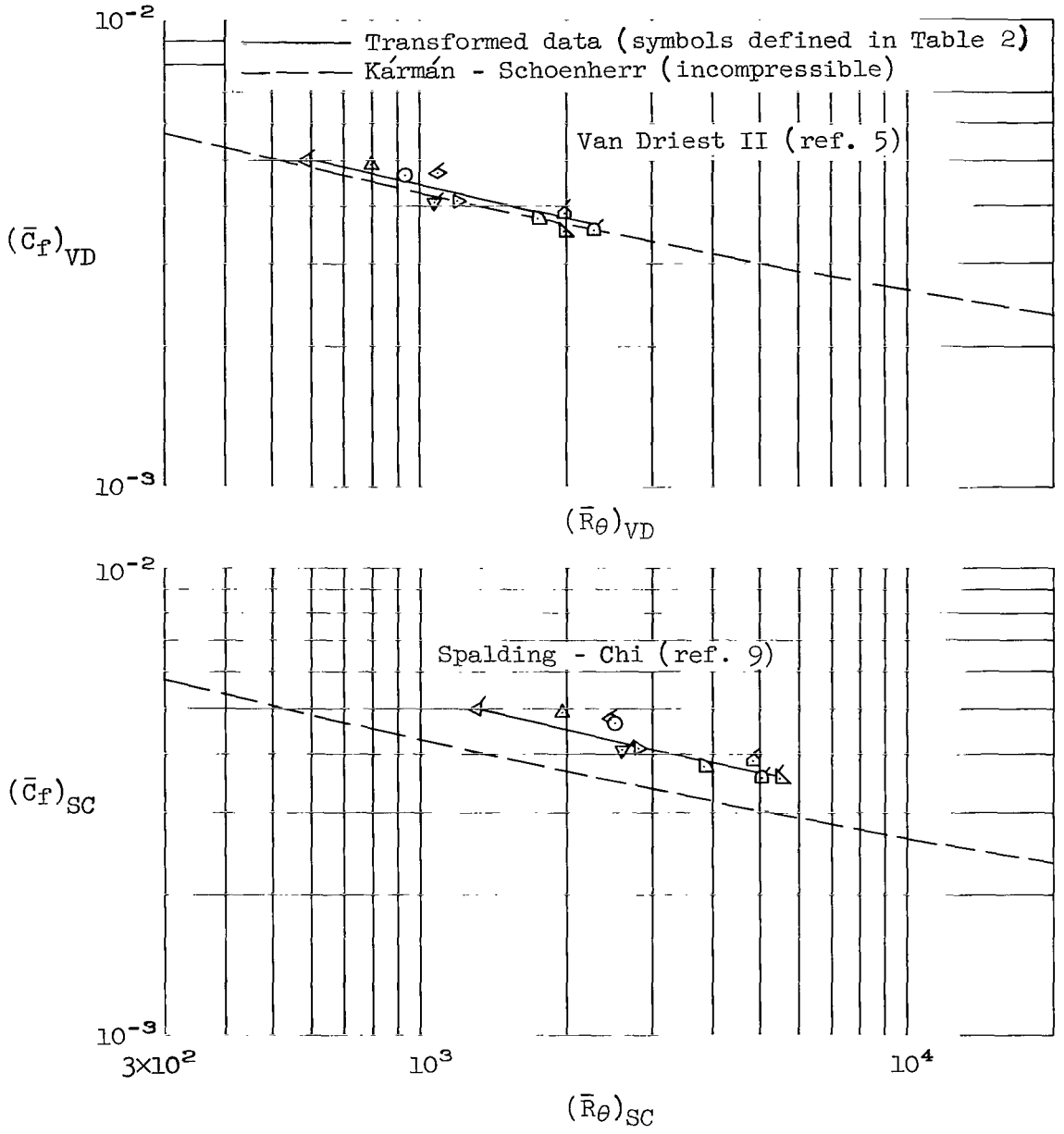

(a) Van Driest II or Spalding and Chi's theories.

Figure 7.- Transformed skin-friction data.

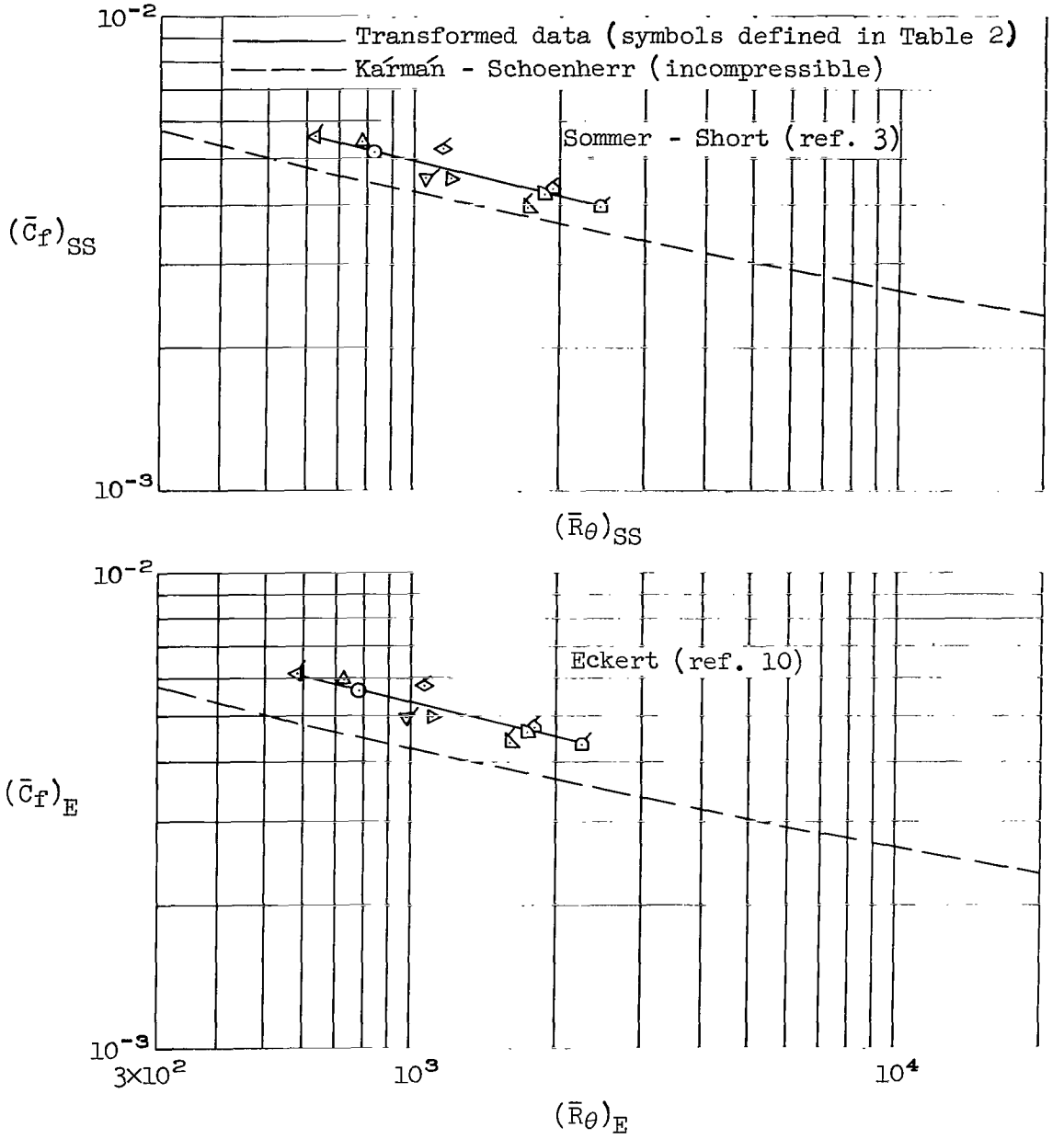

(b) Sommer and Short or Eckert's theories.

Figure 7.- Continued.

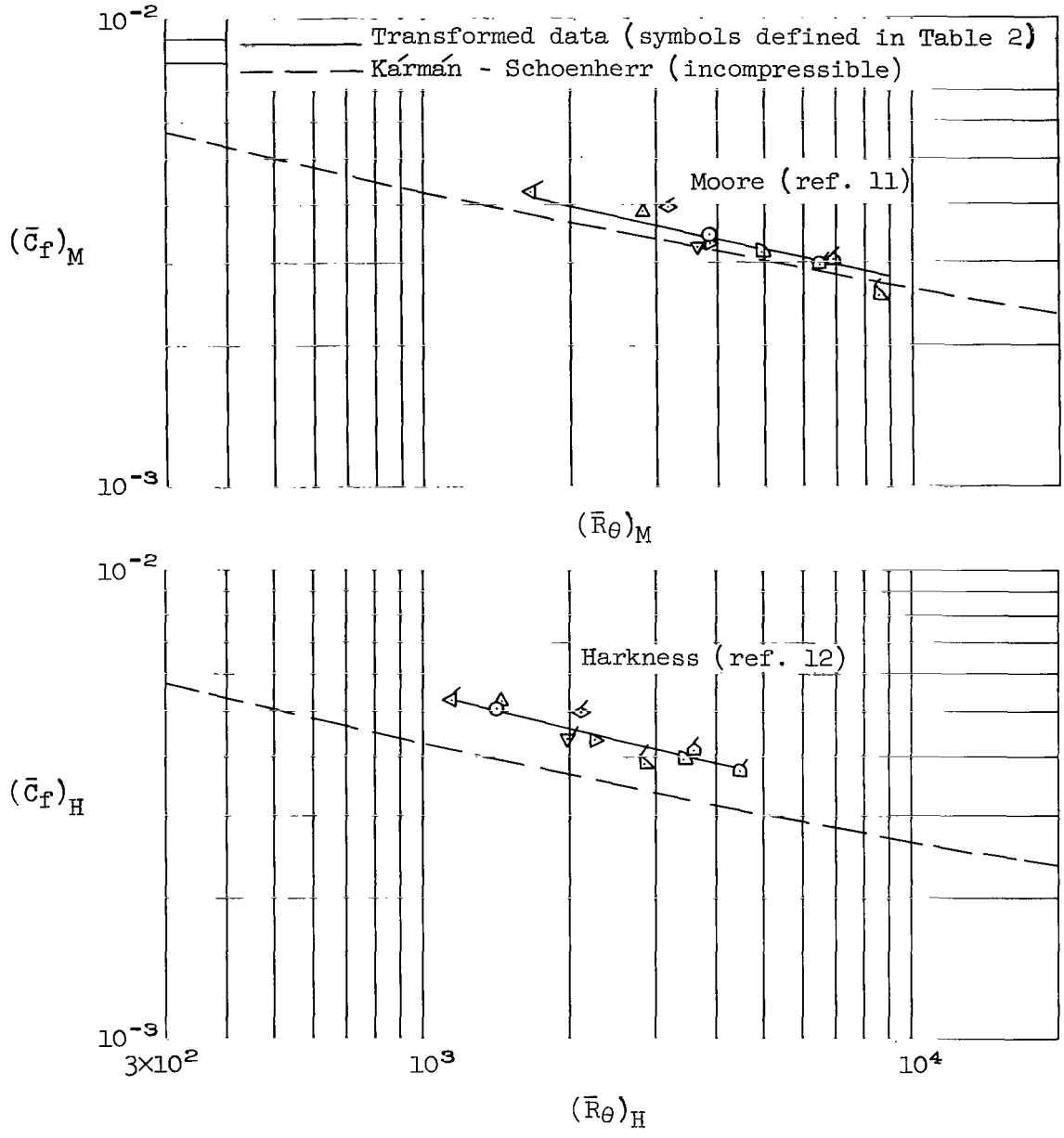

(c) Moore or Harkness' theories.

Figure 7.- Continued.

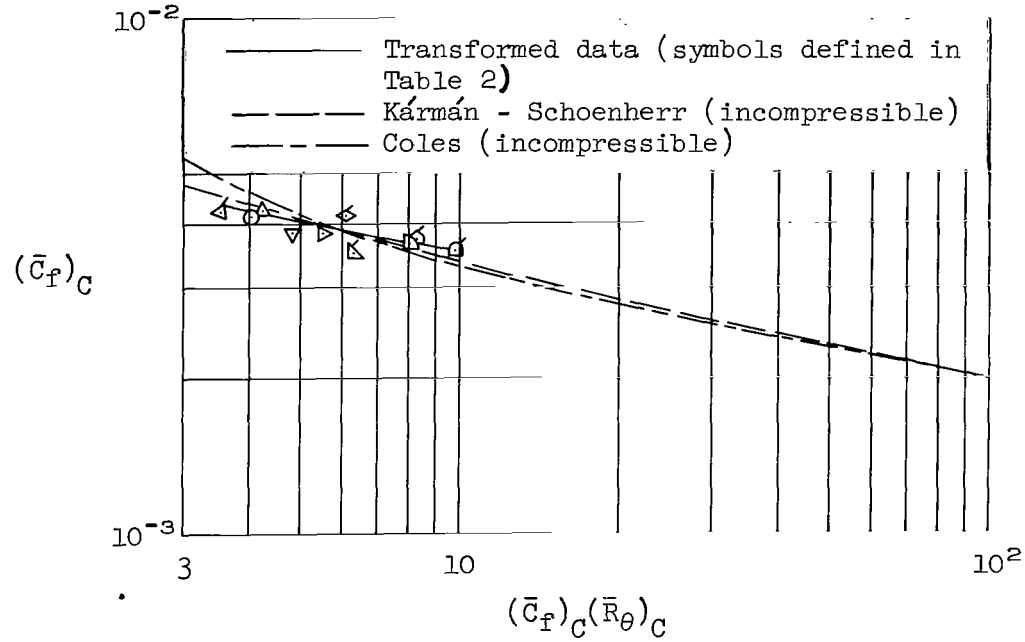

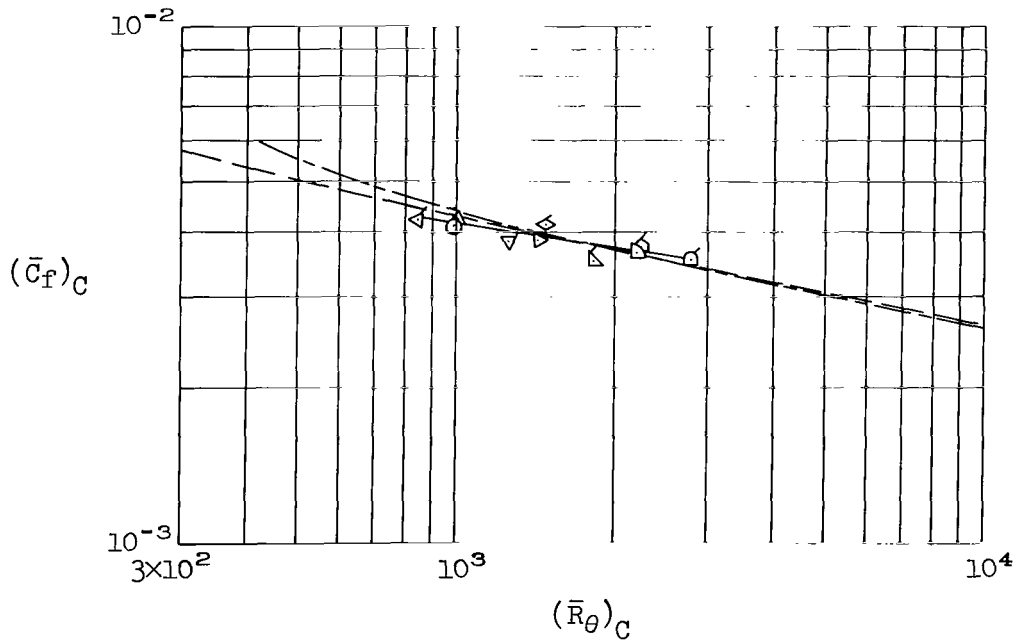

(d) Coles' theory (ref. 13).

Figure 7.- Continued.

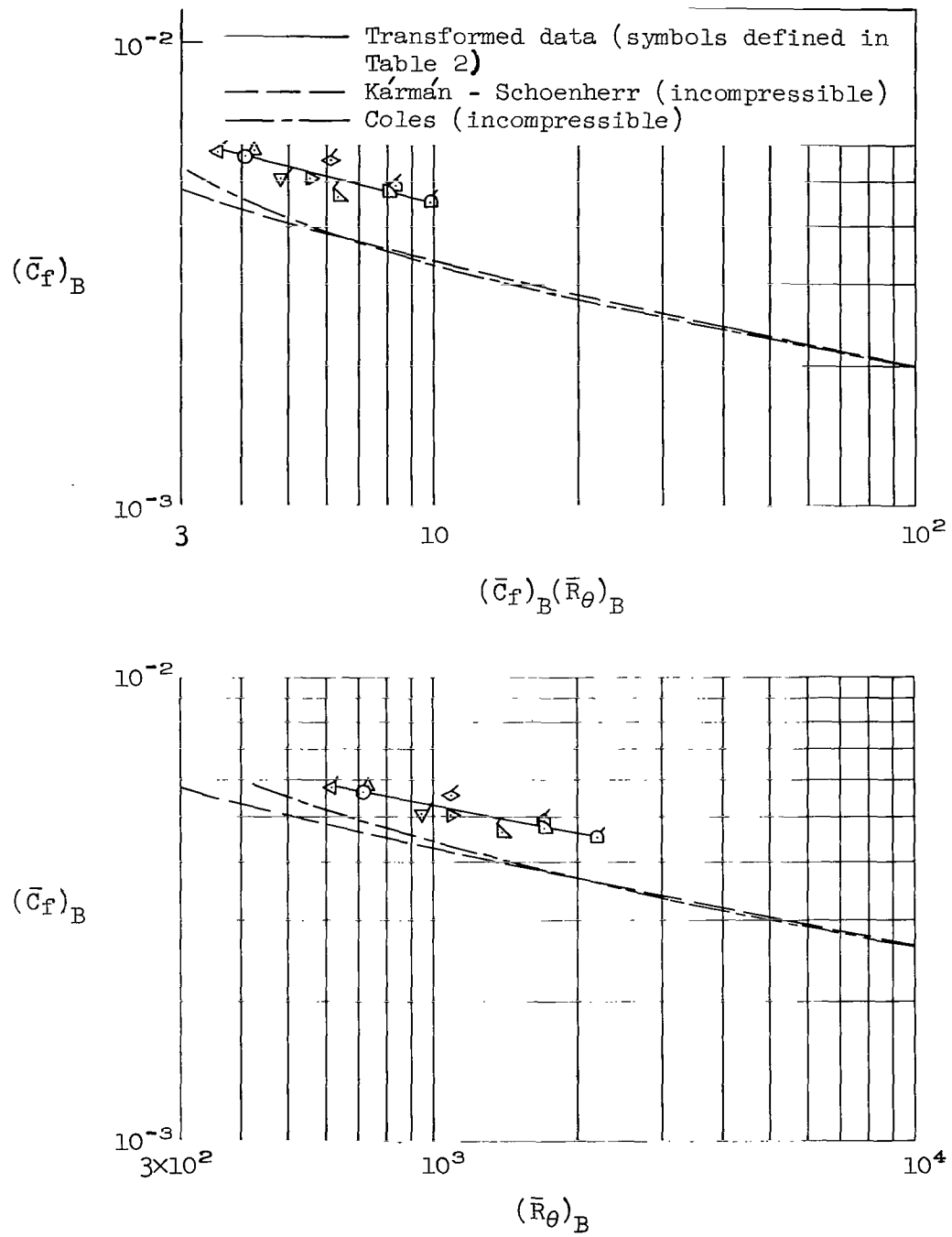

(e) Baronti and Libby's theory (ref. 14).

Figure 7.- Concluded.

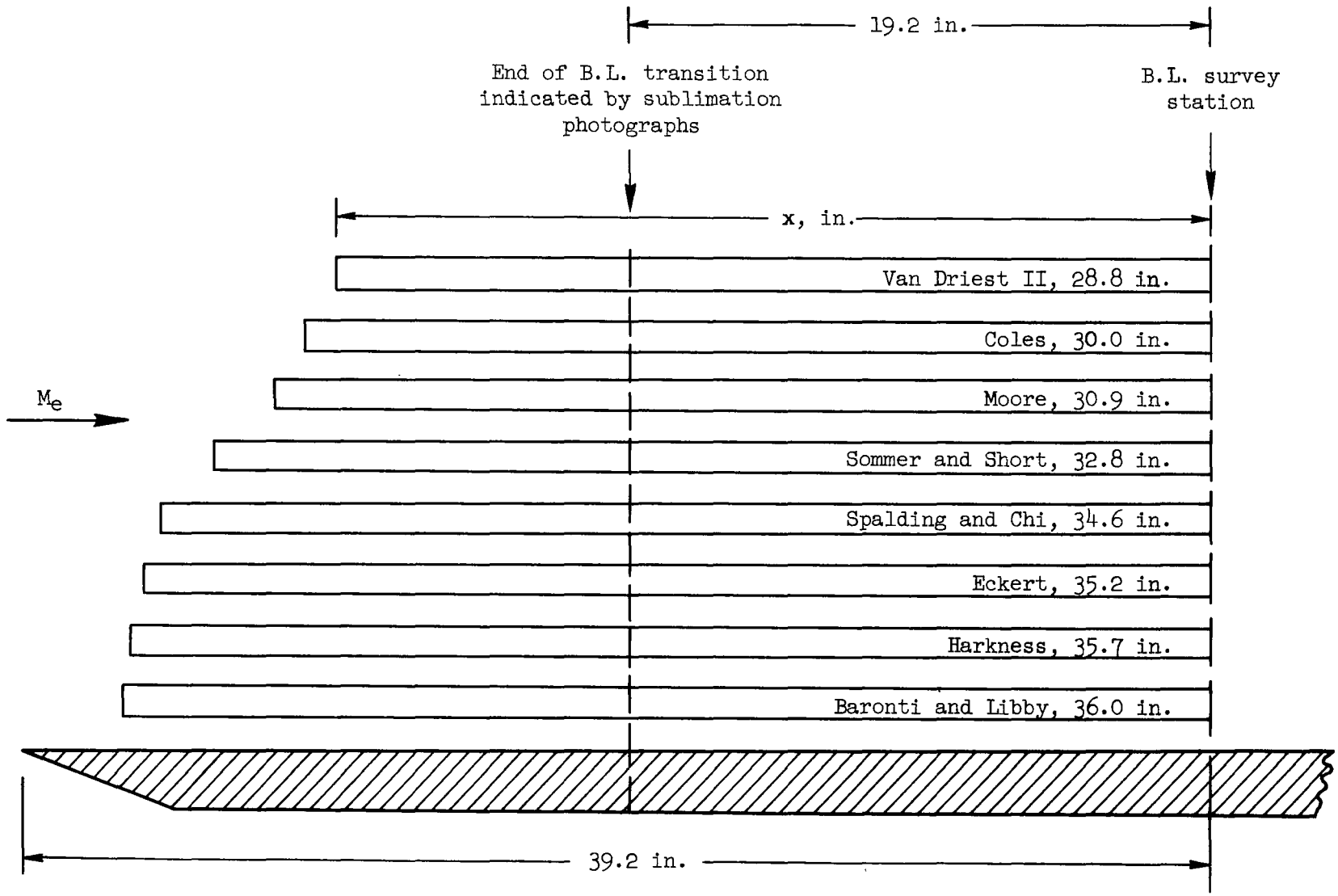

Figure 8.- Virtual origin of turbulent flow calculated from R_θ; natural transition; $U_e/\nu_e = 4.065 \times 10^6 \times ft^{-1}$.

NATIONAL AERONAUTICS AND SPACE ADMINISTRATION
WASHINGTON, D. C. 20546
OFFICIAL BUSINESS

FIRST CLASS MAIL

POSTAGE AND FEES PAID
NATIONAL AERONAUTICS AND
SPACE ADMINISTRATION

ıdeliverable (Section 158
ʏostal Manual) Do Not Return

"The aeronautical and space activities of the United States shall be conducted so as to contribute . . . to the expansion of human knowledge of phenomena in the atmosphere and space. The Administration shall provide for the widest practicable and appropriate dissemination of information concerning its activities and the results thereof."

—NATIONAL AERONAUTICS AND SPACE ACT OF 1958

NASA SCIENTIFIC AND TECHNICAL PUBLICATIONS

TECHNICAL REPORTS: Scientific and technical information considered important, complete, and a lasting contribution to existing knowledge.

TECHNICAL NOTES: Information less broad in scope but nevertheless of importance as a contribution to existing knowledge.

TECHNICAL MEMORANDUMS: Information receiving limited distribution because of preliminary data, security classification, or other reasons.

CONTRACTOR REPORTS: Scientific and technical information generated under a NASA contract or grant and considered an important contribution to existing knowledge.

TECHNICAL TRANSLATIONS: Information published in a foreign language considered to merit NASA distribution in English.

SPECIAL PUBLICATIONS: Information derived from or of value to NASA activities. Publications include conference proceedings, monographs, data compilations, handbooks, sourcebooks, and special bibliographies.

TECHNOLOGY UTILIZATION PUBLICATIONS: Information on technology used by NASA that may be of particular interest in commercial and other non-aerospace applications. Publications include Tech Briefs, Technology Utilization Reports and Notes, and Technology Surveys.

Details on the availability of these publications may be obtained from:

SCIENTIFIC AND TECHNICAL INFORMATION DIVISION

NATIONAL AERONAUTICS AND SPACE ADMINISTRATION

Washington, D.C. 20546